Research Article | Vol. 26, No. 5 | 5 Mar 2018 | OPTICS EXPRESS 5126
Optics EXPRESS

Brillouin optical time domain analyzer sensors assisted by advanced image denoising techniques

HUAN WU,[1,3] LIANG WANG,[1,3,*] ZHIYONG ZHAO,[2] NAN GUO,[2] CHESTER SHU,[1] AND CHAO LU[2]

[1]*Department of Electronic Engineering, The Chinese University of Hong Kong, Shatin, N.T., Hong Kong*
[2]*Department of Electronic and Information Engineering, The Hong Kong Polytechnic University, Kowloon, Hong Kong*
[3]*These authors contributed equally to this work*
**lwang@ee.cuhk.edu.hk*

Abstract: We have experimentally analyzed and compared the performance of Brillouin optical time-domain analyzer (BOTDA) sensors assisted by non-local means (NLM) and wavelet denoising (WD) techniques in terms of measurement accuracy and experimental spatial resolution, respectively. Degradation of the measurement accuracy and experimental spatial resolution after denoising by NLM and WD are observed, which originate from the fact that higher signal-to-noise ratio (SNR) improvement is achieved at the expense of sacrificing the details of BOTDA data, and smaller data sampling point number (SPN) gives rise to insufficient redundant information for denoising. The two parameters degrade to different extents depending on the amount of SNR improvement and SPN adopted in data acquisition. Compared with WD, NLM relies more on the features of the raw data, which makes its performance highly dependent on the level of neighbouring data similarity. Also, for the first time we propose and demonstrate a BOTDA assisted by advanced Block-Matching and 3D filtering (BM3D) denoising technique, which minimizes the degradation of the two parameters even under higher SNR improvement and smaller SPN. BM3D takes the advantage of NLM and WD and utilizes the spatial-domain non-local principle to enhance the denoising in the transform domain, thus it shows the least degradation of measurement accuracy/experimental spatial resolution after denoising. Thus the BOTDA assisted by BM3D maintains the best measurement accuracy/experimental spatial resolution compared with those by NLM and WD. We also show that BM3D has the advantage of temperature independent performance, unlike NLM where the accuracy is affected by the temperature value. We believe BM3D would be an excellent denoising technique for state-of-the-art BOTDA sensors. In addition, this work is also valuable for practical applications of image denoising techniques in BOTDA sensors with respect to the appropriate choice of image denoising techniques, design of SNR improvement and the adoption of SPN to maintain optimal measurement accuracy/experimental spatial resolution/data acquisition speed.

OCIS codes: (060.2370) Fiber optics sensors; (290.5900) Scattering, stimulated Brillouin; (190.4370) Nonlinear optics, fibers.

References and links

1. Z. Zhao, M. A. Soto, M. Tang, and L. Thévenaz, "Distributed shape sensing using Brillouin scattering in multi-core fibers," Opt. Express **24**(22), 25211–25223 (2016).
2. X. Bao and L. Chen, "Recent Progress in Distributed Fiber Optic Sensors," Sensors (Basel) **12**(7), 8601–8639 (2012).
3. A. Motil, A. Bergman, and M. Tur, "State of the art of Brillouin fiber-optic distributed sensing," Opt. Laser Technol. **78**, 81–103 (2010).
4. A. Denisov, M. A. Soto, and L. Thévenaz, "Going beyond 1000000 resolved points in a Brillouin distributed fiber sensor: theoretical analysis and experimental demonstration," Light Sci. Appl. **5**(5), 1–8 (2016).

#315842 https://doi.org/10.1364/OE.26.005126
Journal © 2018 Received 20 Dec 2017; revised 13 Feb 2018; accepted 13 Feb 2018; published 20 Feb 2018

Optics EXPRESS

5. M. A. Farahani, M. T. V. Wylie, E. C. Guerra, and B. G. Colpitts, "Reduction in the Number of Averages Required in BOTDA Sensors Using Wavelet Denoising Techniques," J. Lightwave Technol. **30**(8), 1134–1142 (2012).
6. M. A. Soto, J. A. Ramírez, and L. Thévenaz, "Intensifying the response of distributed optical fibre sensors using 2D and 3D image restoration," Nat. Commun. **7**, 10870 (2016).
7. X. Y. Qian, Z. N. Wang, W. Sun, B. Zhang, Q. H. He, L. Zhang, H. Wu, and Y. J. Rao, "Long-range BOTDA denoising with multi-threshold 2D discrete wavelet," in *Asia-Pacific Optical Sensors Conference (A*POS) (OSA, 2016), paper W4A.24.
8. X. Y. Wang, Z. N. Wang, S. Wang, N. T. Xue, W. Sun, L. Zhang, B. Zhang, and Y. J. Rao, 157 km BOTDA with pulse coding and image processing," in *6th Proc. European Workshops on Optical Fibre Sensors (EWOFS)* (SPIE, 2016), paper 99162S.
9. N. Guo, L. Wang, H. Wu, C. Jin, H. Y. Tam, and C. Lu, "Enhanced Coherent BOTDA System without Trace Averaging," J. Lightwave Technol., in press (2017).
10. X. Qian, X. Jia, Z. Wang, B. Zhang, N. Xue, W. Sun, Q. He, and H. Wu, "Noise level estimation of BOTDA for optimal non-local means denoising," Appl. Opt. **56**(16), 4727–4734 (2017).
11. M. A. Soto, J. A. Ramírez, and L. Thévenaz, "Optimizing Image Denoising for Long-Range Brillouin Distributed Fiber Sensing," J. Lightwave Technol., in press (2017).
12. K. Dabov, A. Foi, V. Katkovnik, and K. Egiazarian, "Image denoising by sparse 3-D transform-domain collaborative filtering," IEEE Trans. Image Process. **16**(8), 2080–2095 (2007).
13. H. C. Burger, C. J. Schuler, and S. Harmeling, "Image denoising: Can plain neural networks compete with BM3D?" in *Computer Vision and Pattern Recognition (CVPR)*, (IEEE, 2012), paper 2392–2399.
14. F. Argenti, A. Lapini, L. Alparone, and T. Bianchi, "A tutorial on speckle reduction in synthetic aperture radar images," IEEE Geosci. Remote S. **1**(3), 6–35 (2013).
15. C. A. N. Santos, D. L. N. Martins, and N. D. A. Mascarenhas, "Ultrasound Image Despeckling Using Stochastic Distance-Based BM3D," IEEE Trans. Image Process. **26**(6), 2632–2643 (2017).
16. L. Fang, S. Li, Q. Nie, J. A. Izatt, C. A. Toth, and S. Farsiu, "Sparsity based denoising of spectral domain optical coherence tomography images," Biomed. Opt. Express **3**(5), 927–942 (2012).
17. L. Shao, R. Yan, X. Li, and Y. Liu, "From Heuristic Optimization to Dictionary Learning: A Review and Comprehensive Comparison of Image Denoising Algorithms," IEEE Trans. Cybern. **44**(7), 1001–1013 (2014).
18. V. Katkovnik, A. Foi, K. Egiazarian, and J. Astola, "From Local Kernel to Nonlocal Multiple-Model Image Denoising," Int. J. Comput. Vis. **86**(1), 1–32 (2009).
19. T. Brox, O. Kleinschmidt, and D. Cremers, "Efficient nonlocal means for denoising of textural patterns," IEEE Trans. Image Process. **17**(7), 1083–1092 (2008).
20. A. Buades, B. Coll, and J. M. Morel, "A non-local algorithm for image denoising," in *Conference on Computer Vision and Pattern Recognition (CVPR)*, (IEEE, 2005), pp. 60–65.
21. S. G. Mallat, "A theory for multiresolution signal decomposition: the wavelet representation," IEEE Trans. Pattern Anal. **11**(7), 674–693 (1989).
22. H. Wu, L. Wang, N. Guo, C. Shu, and C. Lu, "Brillouin Optical Time Domain Analyzer Assisted by Support Vector Machine for Ultrafast Temperature Extraction," J. Lightwave Technol. **35**(19), 4159–4167 (2017).
23. S. Foaleng-Mafang, J. C. Beugnot, and L. Thévenaz, "Optical sampling technique applied to high resolution distributed fibre sensors," in *Proc. Optical Fibre Sensors (OFS)*, (SPIE, 2009), paper 750369.
24. S. Durand and J. Froment, "Artifact free signal denoising with wavelets," in *Proc. Acoustics, Speech, and Signal Processing (ICASSP)* (IEEE, 2001), pp. 3685–3688.
25. A. Signorini, S. Faralli, M. A. Soto, G. Sacchi, F. Baronti, R. Barsacchi, A. Lazzeri, R. Roncella, G. Bolognini, and F. Di Pasquale, "40 km long-range Raman-based distributed temperature sensor with meter-scale spatial resolution," in *Conf. on Optical Fiber Communication(OFC)*, (OSA, 2010), paper OWL2.
26. M. A. Soto, G. Bolognini, and F. Di Pasquale, "Analysis of optical pulse coding in spontaneous Brillouin-based distributed temperature sensors," Opt. Express **16**(23), 19097–19111 (2008).
27. W. Li, X. Bao, Y. Li, and L. Chen, "Differential pulse-width pair BOTDA for high spatial resolution sensing," Opt. Express **16**(26), 21616–21625 (2008).
28. K. Dabov, A. Foi, and K. Egiazarian, "Video denoising by sparse 3D transform-domain collaborative filtering," in *Proc. European Signal Processing Conference (EUSIPCO)* (IEEE, 2007), pp. 145–149.
29. M. Lebrun, "An analysis and implementation of the BM3D image denoising method," Image Process. On Line **2**, 175–213 (2012).
30. L. Alvarez, M. Mejail, and L. Geomez, *Progress in Pattern Recognition, ImageAnalysis, ComputerVision, and Applications*, (Springer, 2012).
31. A. C. Bovik, *Handbook of Image and Video Processing*, 2nd ed. (Academic, 2010).
32. S. Sarjanoja, J. Boutellier, and J. Hannuksela, "BM3D image denoising using heterogeneous computing platforms," in *Conf. on Design and Architectures for Signal and Image Processing (DASIP)*, (IEEE, 2015), pp. 4159–4167.

1. Introduction

Brillouin optical time-domain analyzer (BOTDA) sensors have attracted much interest in the past years due to their capability of distributed monitoring of temperature and strain with

Optics EXPRESS

excellent performance [1–3]. It exploits the temperature and strain dependence of Brillouin scattering in fibers and retrieves the local temperature/strain information by time-domain interrogation using counter-propagating pump and probe waves. However, the performance of BOTDA is limited by the signal-to-noise ratio (SNR) degradation of sensing signals, leading to tradeoffs among key parameters, e.g. spatial resolution, sensing accuracy and sensing distance etc [4]. Trace averaging can be used to improve SNR, but averaging thousands of BOTDA traces to obtain an acceptable SNR is very time consuming. Recently, two denoising techniques, i.e. wavelet denoising (WD) and non-local means (NLM), have been proposed to improve the SNR of BOTDA, and attracted lots of attention as they would not add any hardware complexity [5–11]. In [5] 1-Dimensional WD has been used to improve the SNR and reduce the averaging time by 90%. The sensor performance has been improved by 100 times with the use of 2-Dimensional NLM and WD to remove the noise [6]. By combining WD [7] or NLM [8] with optical pulse coding, 150 km sensing range has been achieved using 16 averages at spatial resolution of 4 m and 8 m, and temperature uncertainty of 1.03°C and 0.7°C, respectively. N. Guo et al have realized a coherent BOTDA without averaging using NLM for denoising [9]. In 2017 a patch-based noise estimation algorithm has been proposed to accurately estimate the noise level for better NLM denoising [10]. In the same year the optimization of NLM has been studied for long-range BOTDA [11]. Since the first demonstration of 2-Dimentional NLM and WD image denoising for BOTDA in 2016 [6], NLM and WD have become two major widely used image denoising methods in the current research of BOTDA sensors.

Although NLM and WD have been widely used and shown excellent denoising performance in BOTDA, the measurement accuracy and experimental spatial resolution after denoising by them are not well studied and compared. In this paper, we firstly analyze and compare the performance of NLM and WD with a focus on the impact of SNR improvement and the data sampling point number (SPN) on the measurement accuracy and experimental spatial resolution. The results show that the measurement accuracy/experimental spatial resolution have larger degradation when higher SNR improvement is achieved and smaller SPN is adopted for data acquisition. Compared with WD, NLM depends more on the features of the raw data especially when the SPN becomes relatively small, and thus it has better performance if the neighbouring data similarity is high.

Also, for the first time we propose and experimentally demonstrate a BOTDA assisted by an advanced image denoising technique, i.e. Block-Matching and 3D filtering (BM3D), with the least degradation of measurement accuracy and experimental spatial resolution even under higher SNR improvement and smaller SPN. BM3D is the first algorithm to simultaneously employ non-local principle based image self-similarity and transform-domain filtering for Additional White Gaussian Noise (AWGN) denoising [12,13]. It has been well applied to many fields such as radar imaging and ultrasound despecking [14,15] and optical tomography image denoising [16]. As BM3D takes the advantage of NLM and WD, it maintains the best measurement accuracy and experimental spatial resolution compared with NLM and WD. Lastly, the temperature response of the denoising performance, the computational complexity and processing speed by BM3D are discussed and compared with those by NLM and WD. To the best of our knowledge this is the first report to reveal that the accuracy of NLM is related to the measurand value while those by WD and BM3D are independent of the measurand value. It is worth mentioning that although there are many other state-of-the-art image denoising approaches developed by the computer science community [17,18], we only focus on NLM, WD and BM3D. This is because NLM and WD are currently two major image denoising methods in BOTDA, and BM3D simply takes the advantage of them to achieve better denoising performance for BOTDA sensors. The discussion of other image denoising methods is out of the scope of this work. We believe this work is helpful for practical applications of image denoising techniques in BOTDA sensors with respect to the appropriate choice of image denoising techniques, design of SNR improvement and the adoption of SPN

Optics EXPRESS

to maintain optimal measurement accuracy/experimental spatial resolution/data acquisition speed in BOTDA sensors.

2. Current NLM and WD based image denoising for BOTDA sensors

2.1 Working Principle and setting of algorithm parameters

The basic idea of NLM is to build a pointwise estimate of the image, and it is a form of weighted averaging over a large window, where the weights are determined by the similarity between neighbouring image patches [19]. The weighted averaging operation in NLM is described as follows. Let $g(x_i)$ be the value of the i th pixel. The estimate of the pixel value f_i after denoising is given by [20]:

$$f_i = \frac{\sum_{j \in N_i} w_{i,j} * g(x_j)}{\sum_{j \in N_i} w_{i,j}} \tag{1}$$

$$w_{i,j} = G_h\left(\left\|\boldsymbol{g}_i - \boldsymbol{g}_j\right\|_2\right) = \exp\{-\frac{1}{h^2}\left\|\boldsymbol{g}_i - \boldsymbol{g}_j\right\|_2\} \tag{2}$$

Here N_i is the set of pixels involved in the averaging process which allows to include pixels within a very large window or even the entire image; $w_{i,j}$ is the weight for the j th pixel in N_i which is determined by the similarity between neighbouring image patches rather than the individual pixel values; $\boldsymbol{g}_i$ denotes a vector of pixel values in a small image patch (e.g. 5×5) and h is the smoothing control parameter which controls the level of denoising. The larger the value of h, the higher the strength of denoising. There are three parameters in NLM required to optimize: similarity window size, search window and smoothing control parameter h. In this work, as the SPN is varied from 4 to 10, we set the similarity window to be the smallest size of 3×3 to ensure there is no detrimental impact induced by NLM on the spatial resolution and the search window to be 13×13 to reduce the computational complexity [11]. We change the smoothing control parameter h to achieve different levels of SNR improvement.

On the other hand, unlike NLM which works in the spatial domain, WD operates in the transform domain using the sparse representations [21]. The denoising procedure includes the following three steps,

1) Decomposition: the noisy image is first decomposed into many subbands by discrete wavelet transform (DWT). A wavelet basis (mother wavelet) such as Haar, Daubechies, Symlets, and Coiflet is selected and the wavelet decomposition of the signal is computed at a level of L.

2) Thresholding: wavelet coefficients smaller than the threshold are considered as noise which are eliminated. In hard thresholding, all wavelet coefficients below the threshold level are set to be zero while those larger than the threshold are kept. The hard thresholding operator τ is defined by:

$$\tau(x) = \begin{cases} x \ \ if \ |x| > \lambda \\ 0 \ \ if \ |x| \le \lambda \end{cases}$$

where λ is the threshold and x is wavelet coefficients after DWT.

3) Reconstruction: the image is reconstructed by inverse DWT where an image with less noise is reconstructed based on the remaining wavelet coefficients of level. L

Optics EXPRESS

For denoising in BOTDA, 1-Dimensional WD [5] and 2-Dimensional WD [6,7] have been employed to improve the SNR. In [5–7], *symlet*7 and *symlet*8 are used as mother wavelet with 4 and 5 levels of decomposition in DWT. In our case, we have tried different mother wavelets and decomposition levels, and finally we utilize mother wavelet of *symlet*7 and decomposition level of 5 with hard thresholding. To achieve different levels of SNR improvement, we vary the threshold value.

2.2 Performance analysis and comparison of two-dimensional NLM and WD

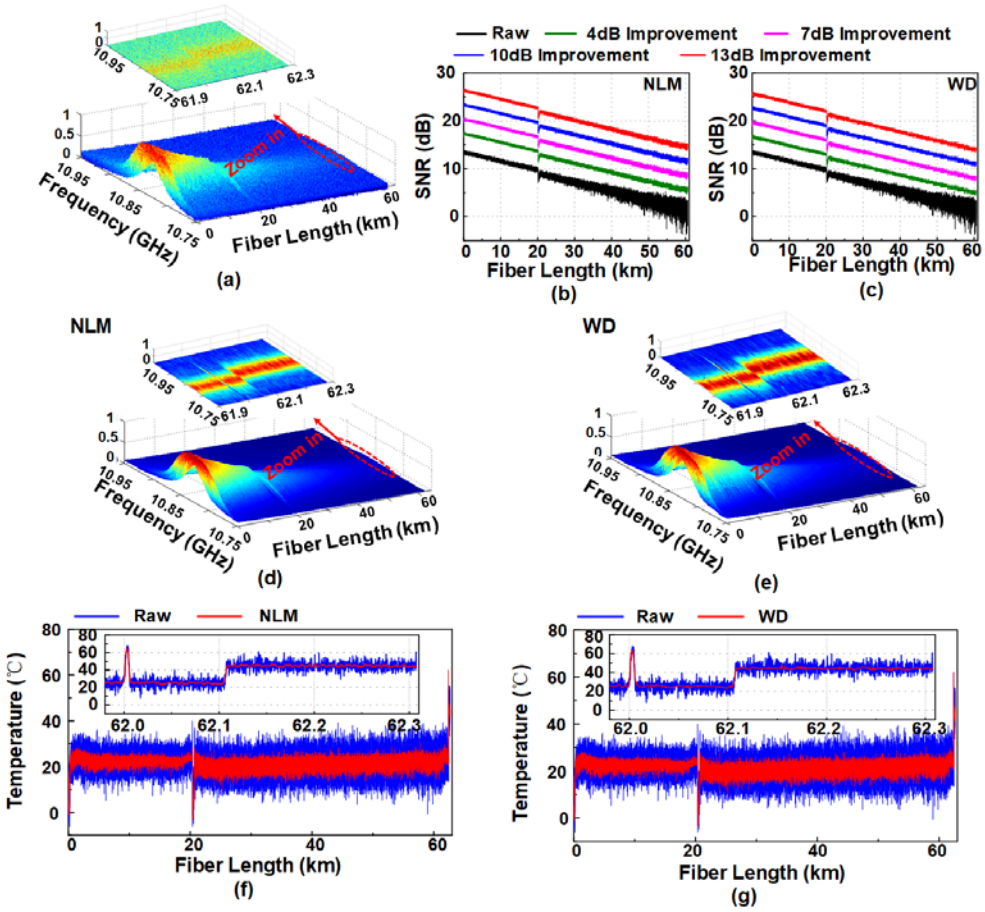

Fig. 1. (a) Measured BGS distribution along FUT without denoising; SNR evolution along FUT for different levels of SNR improvements by (b) NLM and (c) WD; measured BGS and temperature distribution along FUT under SNR improvement of 13dB by (d, f) NLM and (e, g) WD. Inset: zoom-in view around the heated sections. The sampling rate is 500MSample/s, corresponding to SPN = 10 within 2m section.

We use conventional BOTDA setup [22] to measure the Brillouin gain spectrum (BGS) distribution along a 62.3 km fiber under test (FUT), which consists of a ~21 km fiber reel and a ~41 km fiber reel. 20 ns pump pulse width, 16 averaging times and 200 scanning frequencies at a step of 1MHz are used for the measurement. Relatively low averaging times are intentionally adopted to facilitate the achievement of different SNR improvement by image denoising. Two sections of FUT near the fiber end are heated in the following way: a 2m fiber section at the location of 62km is heated to 65°C inside an oven, while the last 200m fiber section is heated to 45°C in another oven. This arrangement imitates practical situations of different temperatures at different locations, which makes the results more generalized. We

Optics EXPRESS

use three data sampling rates on the oscilloscope to collect data, i.e. 500 MSample/s, 300 MSample/s and 200 MSample/s, in order to have 10, 6 and 4 sampling data points collected along a 2m section (i.e. theoretical spatial resolution), respectively. Note that according to [23], the minimum sampling rate to resolve all the changes in the signal is $f_s = 3/\tau$ where τ is the pulse width. Thus, to resolve 2m hot spot with a pulse width of 20ns, the minimum sampling rate should be 150MSample/s. Lower sampling rate gives rise to smaller SPN but faster data acquisition speed. As an example, Fig. 1(a) shows the measured BGS distribution along the FUT without denoising when the sampling rate is 500 MSample/s (i.e. SPN = 10), where the inset is the zoom-in view at the heated sections.

Next, we apply NLM and WD to denoise the same BOTDA data, respectively. In order to guarantee a fair comparison, the performances of NLM and WD are analyzed under the same level of SNR improvement and SPN. In our demonstration, we present four typical levels of SNR improvement, i.e. 4dB, 7dB, 10dB and 13dB, achieved by setting the level of threshold in

NLM and WD. In WD the wavelet threshold is varied from 1.2σ to 3.4σ where σ is the estimated standard deviation of the noise in the raw data, while in NLM the smoothing control parameter h is adjusted from 1.8σ to 10.6σ. Figures 1(b) and 1(c) show the SNR evolution along FUT for different levels of SNR improvement when NLM and WD are used to denoise the raw data in Fig. 1(a), respectively. Figures 1(d) and 1(e) plot the BGS distribution along FUT with SNR improved by 13dB after denoising. Compared with Fig. 1(a), both the 2m heated section and the last 200m heated section are now clearly recognized in Figs. 1(d) and 1(e). After Lorentzian curve fitting, the corresponding temperature distribution is calculated using the BFS-temperature coefficient of the FUT, as shown in Figs. 1(f) and 1(g). Without denoising the temperature uncertainty along the last 200m section is 3.22°C (blue curve); while the uncertainties are reduced to 0.57°C by NLM and 0.55°C by WD (red curves) when the SNR is improved by the same 13dB, respectively.

We analyze the impact of SNR improvement and SPN on the temperature accuracy due to denoising by NLM and WD. Figures 2(a1)-2(a3) show the temperature distribution around the 2m heated section at the location of 62km when NLM is used to denoise the BOTDA traces collected at 500 MSample/s (SPN = 10), 300 MSample/s (SPN = 6) and 200 MSample/s (SPN = 4), respectively. The black squares represent the result without denoising which serves as a reference for comparison. The green rhombuses, pink triangles, blue triangles and red dots depict the results after denoising by NLM when the SNR is improved by 4dB, 7dB, 10dB and 13dB, respectively. The temperature values given inside the figures show the measured average temperature values within the 2m heated section for each case. We can see that under the same SNR improvement the measured temperature gradually deviates from the oven temperature of 65°C when the SPN decreases from 10 to 4, e.g. for 13dB SNR improvement (red dots) the measured temperature changes from 64.17°C to 50.85°C. The smaller the SPN, the worse the temperature accuracy after denoising. The reason is that when smaller SPN is adopted for data collection, the number of similar patches in the raw data that can be used in the weighted averaging process of NLM becomes fewer, resulting in the reduction of neighbouring data similarity and hence the degradation of temperature accuracy. Moreover, under a relatively small SPN, e.g. 4, the measured temperature changes from 61.61°C to 50.85°C when the SNR improvement increases from 4dB to 13dB, as shown in Fig. 2(a2), implying the accuracy degradation under higher SNR improvement. This is because higher SNR improvement is achieved at the expense of sacrificing some details in the data, i.e. using large threshold (the smoothing control parameter h) in NLM. Thus higher SNR improvement gives rise to larger sacrifice of the measurement accuracy if the SPN is relatively small. However, if the SPN is large enough, e.g. 10 in Fig. 2(a1), which offers sufficient neighbouring data similarity for NLM, the measured temperature is kept close to the oven temperature and the accuracy only has little

Optics EXPRESS

degradation regardless of the amount of SNR improvement. On the other hand, the corresponding results for denoising by WD are shown in Figs. 2(b1)-2(b3). Similar to NLM, the temperature accuracy degrades when higher SNR improvement is achieved and smaller SPN is adopted. For WD the BOTDA signals are decomposed by wavelet transform through which the noise usually appears as small coefficients and useful signals appear as large coefficients together with some small coefficients. The elimination of small coefficients in the transform domain removes the noise but also skips some useful details of the signals. When the SPN is small, the percentage of useful sensing information that is lost will increase, resulting in measurement accuracy degradation. Comparing Figs. 2(a1)-2(a3) with Figs. 2(b1)-2(b3), it is found that under the same SNR improvement and SPN, the degradation of temperature accuracy due to denoising by WD is less than that by NLM, especially under smaller SPN. For example, under SNR improvement of 13dB and SPN of 4, the measured temperature with WD is 55.42°C while that with NLM is 50.85°C. This can be explained by the fact that the performance of NLM is strongly related to the features of the raw data. As the temperature of the 2m heated section is far away from that of adjacent unheated section (i.e. room temperature), the neighbouring data similarity in the raw data is insufficient especially when SPN is small, making the accuracy of NLM worse. We will see in the next section that NLM performs better if the 2m section is heated to a lower temperature which results in more neighbouring data similarity. It is worth mentioning that although the hard thresholding function in WD preserves more original signal information [24], it also leads to measurement fluctuations observed around the adjacent regions of the 2m section, as shown in Fig. 2(b), which is due to the discontinuity at the threshold point.

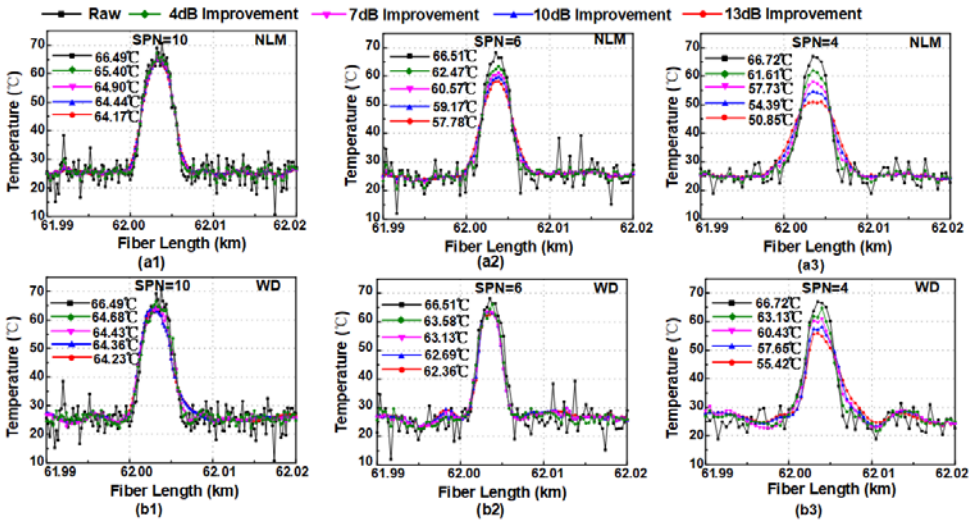

Fig. 2. Temperature distribution around the 2m heated section at the location of 62km with (a1)-(a3) NLM and (b1)-(b3) WD for denoising when SPNs are 10, 6, and 4 within 2m section, respectively. The 2m section is heated to 65°C.

Then we study the impact of SNR improvement and SPN on the experimental spatial resolution due to denoising by NLM and WD. The experimental spatial resolution is defined as the fiber length of the temperature transition region between 10% to 90% of the peak amplitude [25–27]. For the analysis of denoising effect, there should be sufficient sampling data points before and after the temperature transition region to facilitate the denoising process. Thus we use the temperature transition region around the last 200m heated section to calculate the experimental spatial resolution. Figures 3(a1)-3(a3) and Figs. 3(b1)-3(b3) show the temperature distribution around the last 200m heated section when NLM and WD are used for denoising, respectively. The experimental spatial resolution under each SNR

Optics EXPRESS

improvement and SPN is given on the figures. We can see that for both NLM and WD the experimental spatial resolution has larger degradation under higher SNR improvement and smaller SPN. The experimental spatial resolution after denoising gradually deviates from the theoretical value of 2m when the SPN decreases from 10 to 4, e.g. under 13dB SNR improvement (red dots) the spatial resolution degrades from 1.91m to 4.42m by NLM and from 2.14m to 5.5m by WD, respectively. Under a relatively small SPN of 4, when the SNR improvement increases from 4dB to 13dB, the experimental spatial resolution degrades from 3.39m to 4.42m by NLM and from 4.4m to 5.5m by WD as shown in Figs. 3(a3) and 3(b3). In the temperature transition region, there is a large difference among neighbouring data points compared with other regions, and when the SPN is small this difference becomes even larger, which makes the neighbouring data similarity significantly worse. Thus the experimental spatial resolution degrades after denoising by NLM. For WD in addition to the loss of some signal details during the elimination of small coefficients (i.e. noise), another reason for the spatial resolution degradation is the discontinuity at the threshold point in hard thresholding, which results in proneness to volatility in the process of signal reconstruction. The latter one may also cause the fact that under the same condition, WD shows worse experimental spatial resolution than NLM especially when SPN is smaller, which is observed clearly when comparing Figs. 3(a1)-3(a3) with Figs. 3(b1)-3(b3). Higher SNR improvement is achieved at the expense of sacrificing the data originality, which also contributes to the degradation of experimental spatial resolution after denoising.

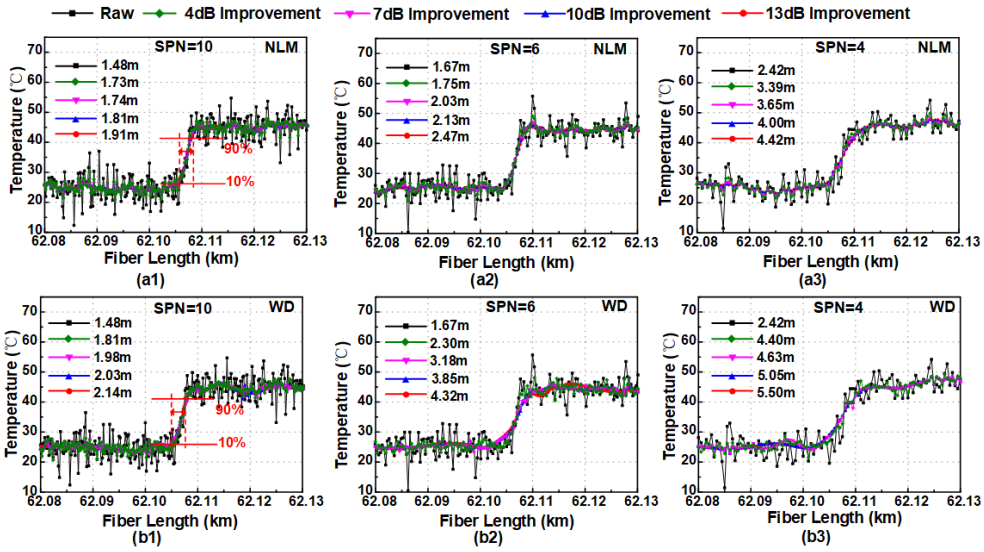

Fig. 3. Temperature distribution around the last 200m heated section with (a1)-(a3) NLM and (b1)-(b3) WD for denoising when SPNs are 10, 6, and 4 within 2m section, respectively. The 200m section is heated to 45°C.

3. Advanced BM3D based image denoising for BOTDA sensors

3.1 Working Principle and setting of algorithm parameters

In this section, we experimentally demonstrate the use of 2-Dimensional BM3D to denoise the BOTDA traces with the least degradation of measurement accuracy and experimental spatial resolution even under higher SNR improvement and smaller SPN. Note that BM3D is a 2D image denoising technique rather than 3D video denoising technique. For 3D video processing the corresponding algorithm is called Video BM3D (VBM3D) [28].

NLM is a spatial-domain filter, which uses the data non-local redundancy from the similarity between neighbouring image patches. WD is a transform-domain filter, which can

easily and efficiently manipulate the information in the transform domain. But WD cannot take advantage of the non-local redundancy present in the image. While BM3D effectively uses both the non-local redundancy and transform-domain filtering for denoising [12]. The algorithm of BM3D includes three main operations: block matching, collaborative filtering and reconstruction. In block matching, BM3D utilizes non-local principle to group similar blocks together to reveal self-similarity of original blocks (or patches) in the image. The "3D" in the name of "BM3D" refers to the operation that the matching blocks of the image are stacked into a 3-Dimensional array, which will be processed by the following collaborative filtering in the transform domain. Collaborative filtering is a special procedure in BM3D, which employs 3D transform and filters the coefficients of the whole 3D array at the same time. Due to the use of self-similarity among blocks, the 3D transform results in more sparser representation of the original blocks, enabling to remove the noise efficiently but still preserves most of the significant details in the original image. Thus BM3D can maintain best measurement accuracy and experimental spatial resolution for denoising in BOTDA compared with NLM and WD.

The three main operations in BM3D in our demonstration are described as follows:

1) Block matching (spatial-domain operation): the whole 3D BGS distribution along the FUT is treated as an image and is processed using sliding window method, where the whole image is divided into several image blocks with a sliding step of N_{step} = 3 pixels from top to bottom, and left to right. Each block has a size of 8×8 pixels. According to the Euclidean distance, similar blocks are searched in the neighbouring area with the currently processed pixel as the center. Based on the suggestion in [29] and our tentative trial on the BOTDA raw data, the search window is restricted to the size of $N_s \times N_s = 39 \times 39$ pixels, and to reduce the complexity of grouping, the maximum number of similar blocks to form a group is set to be $N_{\mathrm{M}} = 16$. Then similar image blocks are stacked over each other to form a 3D array.

2) Collaborative filtering (transform-domain operation): we apply 3D Harr wavelet transform to the 3D array to obtain 3D coefficients. The shared features have large coefficients while the noise is represented by small coefficients. This transform reveals the shared features among blocks efficiently. By hard thresholding, the noise is significantly reduced, while unique details of the original data are kept. To further improve the quality of filtering, Wiener filtering is followed after the hard thresholding. Note that the threshold is varied from 1.5σ to 3.7σ to achieve SNR improvement of 4dB to 13dB.

3) Reconstruction: after inverse transform, noise-reduced blocks in the 3D array are mapped back to their original location with an appropriate weighting of the overlapping blocks.

3.2 Performance analysis of two-dimensional BM3D

In this section, the same raw data collected in Section 2.2 is denoised by BM3D. As an example, Fig. 4(a) shows the SNR evolution along FUT for different levels of SNR improvement when BM3D is used to denoise the raw data in Fig. 1(a). The BGS and corresponding temperature distribution along FUT with SNR improvement of 13dB are given in Figs. 4(b) and 4(c). In Fig. 4(c) the temperature uncertainty at the fiber end is calculated to be 0.55°C (red curve), compared with the uncertainty of 3.22°C without denoising (blue curve).

Optics EXPRESS

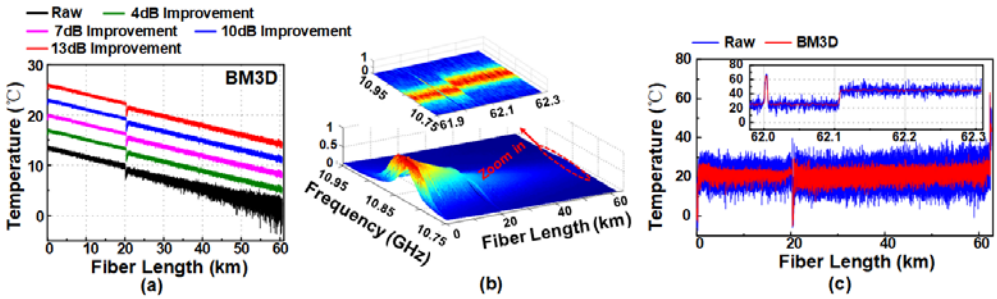

Fig. 4. (a) SNR evolution along FUT for different levels of SNR improvements by BM3D; measured (b) BGS and (c) temperature distribution along FUT under SNR improvement of 13dB. Inset: zoom-in view around the heated sections. The sampling rate is 500 MSample/s, corresponding to SPN = 10 within 2m section.

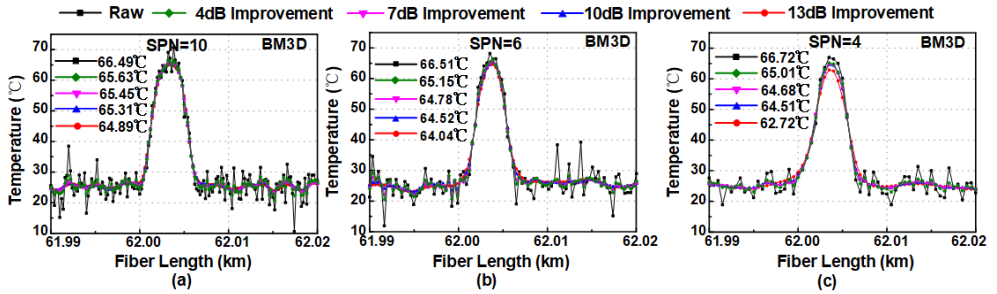

Fig. 5. Temperature distribution around the 2m heated section at the location of 62km with BM3D for denoising when SPNs are (a) 10, (b) 6, and (c) 4 within 2m section, respectively. The 2m section is heated to 65°C.

As comparison to the results by NLM and WD in Figs. 2 and 3, the results by BM3D are presented in Figs. 5 and 6, respectively. Compared with NLM and WD, we can see that the temperature accuracy and experimental spatial resolution after denoising by BM3D have the least degradation when higher SNR improvement is achieved and smaller SPN is adopted. Taking the SPN of 4 as an example, as shown in Fig. 5(c), the measured temperatures are still close to the oven temperature of 65°C even under higher SNR improvement, e.g. 62.72°C under 13dB SNR improvement by BM3D, unlike the cases of NLM and WD in Figs. 2(a3) and 2(b3) where the measured temperatures gradually deviate from the oven temperature when higher SNR improvement is achieved, e.g. 50.85 °C for NLM and 55.42 °C for WD under 13dB SNR improvement. The experimental spatial resolution after denoising by BM3D is 3.86m under SNR improvement of 13dB and SPN of 4, as shown in Fig. 6(c), which is better than 4.42m of NLM and 5.5m of WD. Similar to both NLM and WD, when the SPN is large enough, e.g. 10, the degradation of both temperature accuracy and experimental spatial resolution after denoising by BM3D become negligible, as shown in Figs. 5(a) and 6(a). This is because when SPN is large enough, there is sufficient data that can be used for denoising.

Optics EXPRESS

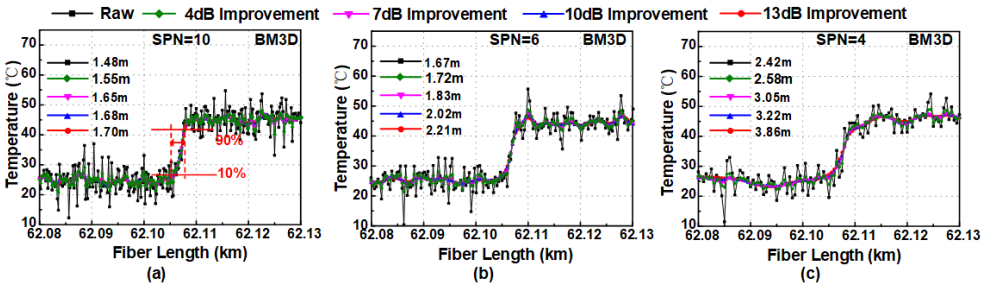

Fig. 6. Temperature distribution around the last 200m heated section with BM3D for denoising when SPNs are (a) 10, (b) 6, and (c) 4 within 2m section, respectively. The 200m section is heated to 45°C.

3.3 Discussion

In this section, we compare the measurement accuracy and experimental spatial resolution by BM3D denoising with those by NLM/WD denoising, respectively. The computational complexity and the processing speed of the three methods are also discussed.

By using the results in Fig. 3 for NLM and WD and Fig. 6 for BM3D, we calculate the measured temperature degradation as a function of SNR improvement under different SPNs, as shown in Fig. 7. To compare the denoising quality of the three techniques, we define the temperature degradation as the difference between the value before (i.e. raw data) and after denoising. Note that since the pump pulse width is 20ns (i.e. theoretical spatial resolution of 2m), we analyze the temperature accuracy within the 2m heated section at the location of 62km. From Fig. 7 we can see that the temperature degradation after denoising by all the three techniques increases as the SNR is improved higher, especially when the SPN is relatively small. However, the one by BM3D increases very slowly, thus it has the least temperature degradation even under higher SNR improvement and smaller SPN, e.g. 4°C degradation under 13dB SNR improvement and 4 SPN compared with 15.87°C by NLM and 11.3°C by WD, as shown in Fig. 7(c). Figures 8 depicts the comparison of experimental spatial resolution among the three techniques, where the degradation is calculated using the results in Fig. 3 for NLM and WD and Fig. 6 for BM3D, respectively. BM3D still has the least degradation for experimental spatial resolution, e.g. 1.44m degradation under 13dB SNR improvement and 4 SPN compared with 2m by NLM and 3.08m by WD, as shown in Fig. 8(c). Figures 7 and 8 confirms again under the same SNR improvement and SPN BM3D maintains the best temperature accuracy and experimental spatial resolution after denoising compared with NLM and WD.

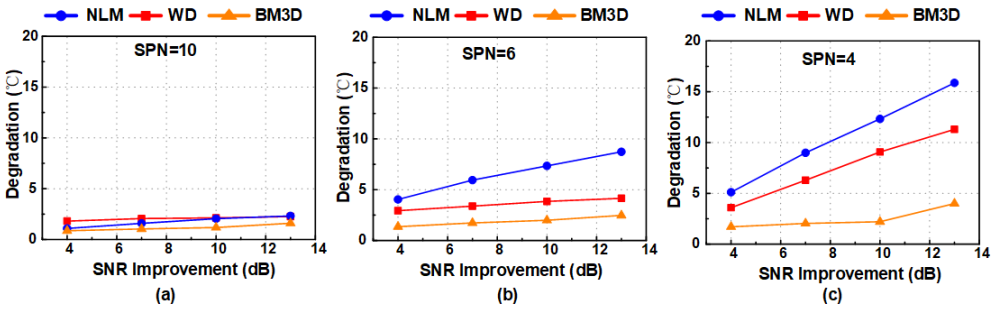

Fig. 7. Temperature degradation as a function of SNR improvement by NLM, WD and BM3D when SPNs are (a) 10, (b) 6, and (c) 4 within 2m section, respectively. The absolute error of temperature is calculated using the results in Fig. 2 for NLM and WD and Fig. 5 for BM3D, respectively. The 2m section is heated to 65°C.

Optics EXPRESS

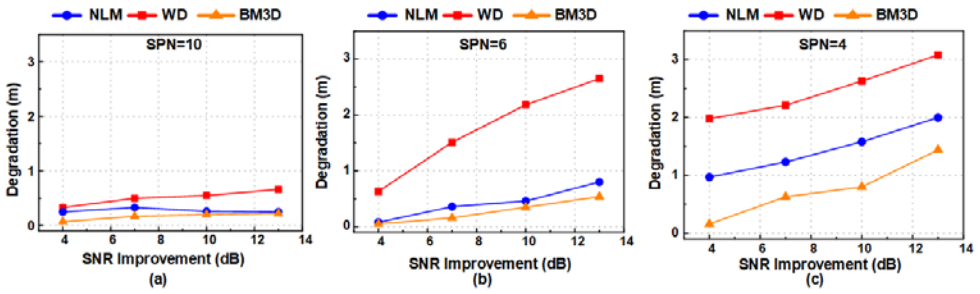

Fig. 8. Degradation of experimental spatial resolution as a function of SNR improvement by NLM, WD and BM3D when SPNs are (a) 10, (b) 6, and (c) 4 within 2m section, respectively. The absolute error of spatial resolution is calculated using the results in Fig. 3 for NLM and WD and Fig. 6 for BM3D, respectively. The 200m section is heated to 45°C.

In all the previous results, the 2m fiber section at the location of 62km is heated to a fixed temperature of 65°C inside one oven. Here, we also change this oven temperature in order to evaluate the temperature dependence of the accuracy after denoising by NLM, WD and BM3D, respectively. The BOTDA traces are collected under the same experimental conditions as those in Section 2.2 except the change of oven temperature from 35°C to 75°C at a step of 10°C. We fix the SNR improvement after denoising by NLM, WD and BM3D to be the same 13dB for fair comparison. Figure 9 plots the measured temperature versus the oven temperature when SPNs are 10, 6, and 4 within 2m section, respectively. The black dashed line indicates the ideal measurement result where the measured temperature is equal to the oven temperature. Under the SPN of 10, the results by the three techniques are all close to the dashed line, which indicates excellent temperature accuracy of all the three techniques when the SPN is large enough to provide sufficient redundant information for denoising. When the SPN is relatively small, e.g. 4, the result by BM3D (orange triangles) is still very close to the dashed line compared with those by NLM (blue dots) and WD (red squares), as shown in Fig. 9(c), which again indicates the best denoising performance by BM3D. On the other hand, it is found that the results of WD and BM3D are always approximately parallel to the dashed line for all SPNs, while that of NLM under smaller SPN gradually deviates from the dashed line when the oven temperature increases. For example under SPN of 4, as shown in Fig. 9(c), when the oven temperature is 35°C, the difference between the measured temperature and oven temperature using NLM, WD and BM3D are 2.29°C, 6.24°C and 1.76°C, respectively. The corresponding values become 18.18°C, 8.8°C and 1.24°C at an oven temperature of 75°C. It implies that the denoising performances by WD and BM3D are independent of temperature while that by NLM is related to the temperature, especially when the SPN becomes smaller. The temperature dependence of NLM performance originates from its operation of weighted averaging using non-local principle based neighbouring data similarity. When the temperature of the 2m heated section (e.g. 35°C) is close to the temperature of adjacent unheated section (i.e. room temperature), the similarity between the data patches of the 2m heated section and adjacent unheated section in the search window is high, giving rise to better temperature accuracy. But when the temperature of the 2m heated section (e.g. 75°C) is away from that of adjacent unheated section, the similarity is low and hence leads to worse accuracy. If the SPN is large enough, e.g. 10, the data points within the 2m section is always sufficient to maintain well similarity for NLM, regardless of the temperature value, as shown in Fig. 9 (a). Therefore, the performance of NLM relies more on the characteristics of the raw data. When the neighbouring data similarity is sufficient NLM performs very well, otherwise it gives worse accuracy than WD, as shown in Figs. 2 and 7 where the 2m section is heated to a temperature (65°C) away from that of the adjacent unheated section. Note that in Ref [11]. the 2m hot-spot is heated to a temperature of around 40°C, thus NLM performs well. For BM3D, although the non-local principle is used in block

Optics EXPRESS

matching, the collaborative filtering in the transform domain rather than the weighted averaging like NLM is applied to remove the noise, making its performance independent of the temperature.

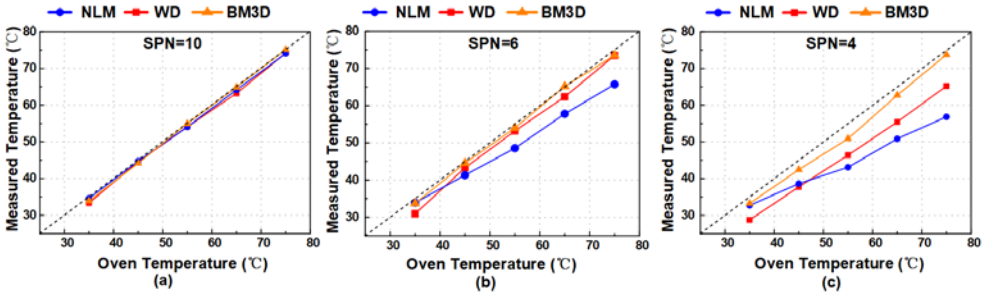

Fig. 9. Measured temperature versus the oven temperature when SPNs are (a) 10, (b) 6, and (c) 4 within 2m section, respectively. The 2m section at the location of 62km is heated to 35°C, 45 °C, 55 °C, 65 °C and 75 °C, respectively. The SNR improvement is the same 13dB after denoising by NLM, WD and BM3D, respectively.

Finally we analyze the computational complexity of BM3D, and compare it with NLM and WD. Here an image of size $M \times N$ is used as an example for the analysis of complexity. For 2-dimensional NLM with a search window of size $\sqrt{P} \times \sqrt{P}$ and similarity window of size $\sqrt{Q} \times \sqrt{Q}$, it gives a computational complexity of $O(M \cdot N \cdot P \cdot Q)$ [30]. The computational complexity of L level 2-Dimensional WD is $O(M \cdot N \cdot L)$ [31]. While for 2-Dimensional BM3D, the computational complexity is $O((C_{T_{3D}} + \frac{N_M \cdot N_s^2}{N_{step}^2}) \cdot N \cdot M)$, where $C_{T_{3D}}$ denotes the computational complexity of 3D transform [12]. We can see that the computational complexity of WD is the simplest while that of BM3D is the most complicated due to its combination of spatial-domain and transform-domain processing. Then we evaluate the processing speed of each algorithm, which is related to their computational complexity. For each algorithm we use the single-thread implementation on a computer with a CPU of Intel i7-5960X, 8 physical processing cores, and 32GB random-access memory (RAM). The processing time is recorded for denoising the collected BOTDA raw data in Fig. 2(a), which contains 200×311500 data points (i.e. 200 scanning frequencies, 62.3km long fiber and 500MSample/s sampling rate). With the SNR improved by 13dB, the processing time by NLM, WD and BM3D are 3.7min, 4.8s and 9.1min, respectively. We can see that BM3D requires more time for denoising as it is more complicated compared with NLM and WD. However, this time can be reduced by further optimization of the algorithm. Moreover, the processing speed of BM3D can also be greatly accelerated by multi-thread implementation using a graphics processing unit (GPU). According to [32], the speed of BM3D can be boosted by 7.5 times using GPU, which implies the time will be reduced to 1.2min for our case. NLM can be boosted too. Note that for traditional averaging method to achieve the same SNR improvement, the big increase of the averaging times will not only result in significant increase of the measurement time [5, 11], but also extra cost on upgrading the hardware to realize large averaging times.

4. Conclusion

We have experimentally studied the impact of SNR improvement and SPN on the measurement accuracy/experimental spatial resolution after denoising by NLM and WD, respectively. After denoising, the degradation of both the temperature accuracy and experimental spatial resolution has been observed, and is found to be dependent on the values

Optics EXPRESS

of SNR improvement and SPN for data acquisition. When the SPN is large enough at high data sampling rate, the degradation is negligible because there is sufficient redundant information for denoising. In comparison, when the SPN is not so large at low data sampling rate, the two parameters have larger degradation under higher SNR improvement and smaller SPN. Higher SNR improvement is achieved at the expense of sacrificing the data originality, which results in the loss of signal details, especially when the SPN is small. NLM employs the weighted averaging based on the data non-local redundancy to minimize the noise, thus its performance degrades as the neighbouring similarity of the BOTDA traces is reduced, especially when small SPN is adopted for data collection. While in WD the removal of the noise in the transform domain also sacrifices some useful details of the signal, which gives rise to the performance degradation. Compared with WD, NLM relies more on the features of the raw data, and thus it produces better performance when the neighbouring similarity of the raw data is high. The hard thresholding function in WD preserves more original signal information but it also generates measurement fluctuations after the signal reconstruction. Therefore, to use WD or NLM for denoising, it is necessary to carefully design the amount of SNR improvement and SPN for data collection in order to maintain acceptable performance.

To reduce the performance degradation under higher SNR improvement and smaller SPN we have proposed and demonstrated for the first time the use of advanced BM3D to denoise the BOTDA traces. As BM3D effectively combines the advantages of spatial-domain non-local principle in NLM and transform-domain sparse representation in WD, it gives rise to the least sacrifice of measurement accuracy/experimental spatial resolution after denoising. Thus compared with NLM and WD, BM3D maintains the best measurement accuracy and experimental spatial resolution.

Furthermore, we also show that the performance of BM3D is independent of temperature, while the accuracy by NLM is affected by the temperature value due to its weighted averaging operation based on non-local principle. Although BM3D has higher computational complexity and requires more processing time compared with NLM and WD, its processing speed can be significantly enhanced by multi-thread implementation using a GPU. Without the need of any hardware modifications image denoising can provide an efficient and powerful way of improving the performance of BOTDA sensors. Especially for cost-effective industrial applications, image denoising is highly attractive as it can be integrated into any existing distributed fiber sensor systems with no hardware complexity. Thus we believe BM3D will be a very promising denoising technique for high-performance distributed fiber sensors.

Acknowledgement

Research Grants Council of Hong Kong (RGC) project: CUHK GRF 14206614, 14238816, 14209517, PolyU 5208/13E; and National Natural Science Foundation of China: NSFC 61377093, 61435006.